



A comparative analysis between viscoacoustic equations based on different rheological models using Devito

^{1,2}Nogueira P.; ²Silva, L.M.; ²Jesus, L.R.S.; ¹Porsani, M. (¹UFBA/INCT-GP, ²SENAI CIMATEC)

Copyright 2022, SBGf - Sociedade Brasileira de Geofísica.

Este texto foi preparado para a apresentação no IX Simpósio Brasileiro de Geofísica, Curitiba, 4 a 6 de outubro de 2022. Seu conteúdo foi revisado pelo Comitê Técnico do IX SimBGf, mas não necessariamente representa a opinião da SBGf ou de seus associados. É proibida a reprodução total ou parcial deste material para propósitos comerciais sem prévia autorização da SBGf.

Abstract

Most seismic imaging applications still consider the subsurface as a perfect acoustic or elastic medium, ignoring the viscosity of rocky materials. That viscosity converts part of the mechanical energy of seismic waves into heat, affecting the amplitude and phase of the wavefield. In this work, we derive, implement and analyze a set of forward and adjoint viscoacoustic equations based on the Maxwell, Kelvin-Voigt (KV), and standard linear solid (SLS) rheological models. For this implementation, we used Devito - a domain-specific language (DSL), and code generation framework to design highly optimized finite difference kernels for use in inversion methods. We analyzed the attenuating behavior, comparing each equation's dissipation and dispersion effects in these models, both forward modeling equations through comparisons between snapshots, seismograms, and traces, and adjoint equations through RTM images.

Introduction

During the seismic wave propagation in the subsurface, the conversion of mechanical energy into heat occurs due to the rock's viscosity (Walcott 1970). In seismic exploration, the subsurface has still been considered an ideal elastic/acoustic medium, disregarding the attenuating effects. In practice, the propagation of seismic waves in the subsurface is different from propagation in an ideal solid. The acoustic/elastic wave equation is not sensitive enough to describe propagation in these more complicated media. Generally, the viscosity of materials in the subsurface causes energy dissipation and consequently a decrease in amplitude, in addition to modifying the frequency content of waves. This phenomenon of wave energy dissipation is called seismic absorption or attenuation.

Rheological models have been developed to describe the attenuation effects during seismic wave propagation. Viscoacoustic models can also be simulated using wave equations in the time domain by superimposing a series of relaxation mechanisms (Schiessel et al. 1995). The Maxwell model that combines a spring (responsible for the elastic behavior of the material) and a dashpot (attenuating element) in series. This model considers that the force applied to both elements is the same; however, the elongation (strain) is different since the extension in the spring is instantaneous, which does not occur in the dashpot. The quality factor (Q) is directly proportional to

the frequency, its damping being much more substantial at low frequencies (Carcione, 2014). Another mechanical model commonly used to describe anelastic effects is the KV model, which represents the combination of a spring and a dashpot connected in parallel. The deformation in both elements is the same. However, the force is different, and its behavior is better defined by a creep function, the reciprocal relaxation function in the frequency domain. Its quality factor Q is inversely proportional to the frequency. Consequently, there is a more significant attenuation in the high-frequency content. An SLS element consists of a series combination of a spring and a KV model. The stress-strain relationships are obtained from the SLS model as a temporal convolution, which requires storage for the wavefields for all timesteps. However, this temporal convolution can be replaced by the introduction of an auxiliary memory variable (Carcione et al. 1988).

In this work, we compare wavefields, seismograms, and RTM images for geological media with different complexities. The equations based on the SLS, Maxwell and KV models take as reference the works of Carcione (2014), Dutta & Schuster (2014), Deng & McMechan (2007) and Ren et al. (2014). We implement all equations using Devito, a DSL used to solve modeling and seismic inversion problems in a high-performance computational environment (Kukreja et al., 2018; Louboutin et al., 2018).

Forward and adjoint modeling equations

The construction of mechanical models is based on two elements (springs and dashpots) connected in series, parallel, or a combination in series and parallel. The spring represents the elastic behavior, whereas the dashpot (represented by a cylindrical piston filled with viscous liquid) represents the dampening behavior.

The viscoacoustic equations based on rheological models is originated from the *stress-strain* relationship:

$$\sigma = \frac{\partial \psi}{\partial t} * \varepsilon = \psi * \frac{\partial \varepsilon}{\partial t}, \quad (1)$$

σ is the stress, ε is the deformation, and ψ is the relaxation function. Moreover, we have the following relation

$$\frac{\partial \varepsilon}{\partial t} = \nabla \cdot \mathbf{v}, \quad (2)$$

with \mathbf{v} being obtained by motion equation

$$\frac{\partial \mathbf{v}}{\partial t} = \frac{1}{\rho} \nabla \sigma, \quad (3)$$

where \mathbf{v} is the particle velocity, and ρ is the density.

Maxwell model

The relaxation function for Maxwell model is defined as:

$$\psi = M_U e^{(-t/\tau)} H(t) \quad (4)$$

where M_U is the elasticity constant of the unrelaxed spring, $H(t)$ is the Heaviside function, and $\tau = \eta/M_U = \omega_0 Q$ is the relaxation time, being η the viscosity and Q the quality factor. From Equation 1 with some operations, we obtain the equations system:

$$\begin{cases} \frac{\partial p}{\partial t} + \kappa \nabla \cdot \mathbf{v} + \frac{\omega_0}{Q} p = \int S(\mathbf{x}_s, t) \\ \frac{\partial \mathbf{v}}{\partial t} + \frac{1}{\rho} \nabla p = 0, \end{cases} \quad (5)$$

where κ is the bulk modulus and $\omega_0 = 2\pi f_0$ is the angular frequency, being f_0 the dominant frequency.

The adjoint-state method (Plessix, 2006) was used to computation the adjoint equation of the forward modeling operator, applying the adjoint operation in the equation 5, we have:

$$\begin{cases} \frac{\partial q}{\partial t} + \nabla \cdot \frac{1}{\rho} \mathbf{u} - \frac{\omega_0}{Q} q = -\Delta d, \\ \frac{\partial \mathbf{u}}{\partial t} + \nabla \kappa q = 0. \end{cases} \quad (6)$$

Kelvin-Voigt model

The relaxation function to KV model is determined as:

$$\psi = M_R H(t) + \eta \delta(t), \quad (7)$$

where M_R is the elasticity constant of the relaxed spring, η is the viscosity, $H(t)$ and $\delta(t)$ are the Heaviside and Dirac delta functions, respectively.

Again, starting from Equation 1, using the relaxation function (Equation 7) and following some steps, we get:

$$\begin{cases} \frac{\partial p}{\partial t} + \kappa \nabla \cdot \mathbf{v} - \eta \nabla \cdot \frac{1}{\rho} \nabla p = \int S(\mathbf{x}_s, t), \\ \frac{\partial \mathbf{v}}{\partial t} + \frac{1}{\rho} \nabla p = 0. \end{cases} \quad (8)$$

being $\eta = \tau \kappa$ with $\tau = (\omega_0 Q)^{-1}$, where κ, η, τ are the bulk modulus, viscosity, and relaxation time, respectively.

After applying the adjoint-state method in equation 8, we obtain:

$$\begin{cases} \frac{\partial q}{\partial t} + \nabla \cdot \frac{1}{\rho} \mathbf{u} + \nabla \cdot \frac{1}{\rho} \nabla \eta q = -\Delta d, \\ \frac{\partial \mathbf{u}}{\partial t} + \nabla \kappa q = 0. \end{cases} \quad (9)$$

SLS model

The SLS model is the most realistic, consisting of a KV model connected in series with a spring. The relaxation function of this model is defined by

$$\psi = M_R \left[1 - \left(1 - \frac{\tau_\varepsilon}{\tau_\sigma} \right) e^{-t/\tau_\sigma} \right] H(t) \quad (10)$$

Thus, starting of Equation 1, using Equation 10, and following some steps, we have

$$\begin{cases} \frac{\partial p}{\partial t} + \kappa(\tau + 1)(\nabla \cdot \mathbf{v}) + r_p = \int S(\mathbf{x}_s, t), \\ \frac{\partial \mathbf{v}}{\partial t} + \frac{1}{\rho} \nabla p = 0, \\ \frac{\partial r_p}{\partial t} + \frac{1}{\tau_\sigma} [r_p + \tau \kappa(\nabla \cdot \mathbf{v})] = 0, \end{cases} \quad (11)$$

where $\rho(\mathbf{x})$ is the density at position \mathbf{x} , $\kappa = \kappa(\mathbf{x})$ is the Bulk modulus, $\mathbf{v} = \mathbf{v}(\mathbf{x}, t)$ is the particle velocity vector, $S = S(\mathbf{x}_s, t)$ is the source at position \mathbf{x}_s . The symbol * represents

a convolution operation, which describes the dissipation mechanism in a viscoacoustic medium in Equation 1. $\tau = \tau_\varepsilon/\tau_\sigma - 1$ represents the magnitude of Q . τ_ε e τ_σ are, respectively, the relaxation time *stress* and *strain*, given by:

$$\tau_\sigma = \frac{\sqrt{Q^2 + 1} - 1}{2\pi f_0 Q} \quad \text{and} \quad \tau_\varepsilon = \frac{\sqrt{Q^2 + 1} + 1}{2\pi f_0 Q}. \quad (12)$$

Applying adjoint-state method in equation 11:

$$\begin{cases} \frac{\partial q}{\partial t} + \nabla \cdot \frac{1}{\rho} \mathbf{u} = -\Delta d, \\ \frac{\partial \mathbf{u}}{\partial t} + \nabla(\tau + 1)\kappa q + \nabla \kappa \frac{\tau}{\tau_\sigma} r_q = 0, \\ \frac{\partial r}{\partial t} - \frac{1}{\tau_\sigma} r - q = 0. \end{cases} \quad (13)$$

Numerical experiments

We conduct modeling and migration experiments for equations derived from the Maxwell, KV, and SLS models. We use geological models of different complexities. The simplest models we tested were for one and two layers, in which we compared the wavefields and seismograms for each forward modeling equation. We perform an RTM using the adjoint equations of each rheological model. The observed input data for RTM to all cases were generated with the viscoelastic equation based on the work of Robertsson et al. (1994).

v and Q constant models

Figure 5 shows the effect of amplitude and phase attenuation of a seismic wave that propagates in a homogeneous medium of constant velocity for different values of Q and different equations. An integrated Ricker function with a peak frequency of 20 Hz was used as a source, injected in the model's center.

The wavefront in Figure 5 compares with $Q = 20$ and $Q = 50$ concerning the acoustic case, which is pretty similar for small propagation timesteps. However, as the propagation time increases and the wavefield moves to greater distances, the attenuation becomes more pronounced, especially for experiments with $Q = 20$. It is possible to see in Figure 5e and 5f simulated with Maxwell equations have higher dissipative power than approaches based on KV and SLS equations due to a pronounced wavefront amplitude drop.

Two-layer model

The two-layer model (Figure 1) is used to show the stability of the viscoacoustic modeling for a medium with high-velocity contrast and Q factor, as well as to highlight the reflection and transmission phenomena in Figure 6.

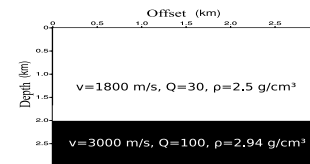


Figure 1 – Two-layer model parameters. Top layer: $v = 1800$ m/s and $Q = 30$. Bottom layer: $v = 3000$ m/s and $Q = 100$.

Figure 6c presents the time instants of a wave field propagated up to 0.5 s time. At first glance, it is worth noting that the generated wavefronts with the Maxwell and KV equations present more evident energy dissipation than those of the SLS. To make a deeper analysis, we take a trace at the 1.5 km offset, as illustrated by the dash in Figure 6c, to the wavefront of all equations and put them together in a comparison shown in Figure 6d. Observing these comparisons, it is easy to conclude that the green dashed line representing the SLS model is the only one that presents a phase shift concerning the acoustic case, regardless of the order of the equation used.

Figure 6a shows a modeled seismogram with a source in the center at the surface. According to the reflection indicated by the red arrow, the substantial drop in amplitude occurs in all viscoacoustic equations. However, the SLS model is the one that has the lowest loss, especially the Maxwell model, which ends up with an almost imperceptible reflection. To more accurately observe the effects observed in the seismograms, we compared the traces taken at the 1 km position, as dashed in Figure 6a, where they are in Figure 6b. In this image, the green trace has a sizeable temporal displacement concerning the others, thus indicating that the SLS models have a strong dispersion. Still analyzing the green trace, there is also a marked loss of amplitude concerning the reference acoustic. The KV and Maxwell EVAs, on the other hand, showed only energy dissipation, with Maxwell being extremely sensitive to low Q factor values.

Marmousi

Figure 2a shows the velocity model, the values varies of 1500 m/s to 5500 m/s. The Q model was calculated by empirical equation $Q = 3.516 \times v^{2.2} \times 10^{-6}$ (Li, 1993). Using the Gardner relation (Gardner et al., 1974), we obtained the density model. In addition, we calculated an approximation of reflectivity (Figure 2b). These models have $9.2 \times 3 \text{ km}^2$, were discretized with $n_x = 369$ and $n_z = 375$ samples, in a mesh of $\Delta x = 25 \text{ m}$ and $\Delta z = 8 \text{ m}$. The total recording time was 4 s, with frequency peak of 12 Hz, considering 5716 samples at a sampling interval $\Delta t = 0.7 \text{ ms}$.

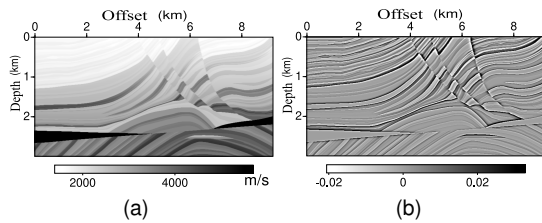


Figure 2 – Marmousi model: velocity (a) and reflectivity (b).

We performed numerical simulations for the seismogram with the source located at 4.7 km and receivers scattered on the surface. The arrows indicated in Figure 7a shows a decrease in the amplitudes of the seismic events. Analyzing the central region of the seismograms in the time interval from 1.5 to 2.5 s presents a more significant attenuation than the other regions, mainly for the Maxwell and KV viscoacoustic equations. The traces taken at 3.75 km offset are shown in Figure 7b, examining the green trace in the SLS viscoacoustic equation we can see a temporal displacement does not occur in the remaining

traces, indicating that only phase dispersion occurs for this equation.

Figure 8a shows snapshots at times 0.7 e 1.2 s. We note that for the shorter times, there is no noticeable distortion of the wavefronts. For longer times, in general, a slight loss of amplitude, especially in the central region of the model. We also analyzed the trace at the 4.6 km offset, as indicated by the dashed line in Figura 8a. Figure 8b show the comparison between the traces for the wavefields at time 0.7 s and the wavefields at time 1.2 s, respectively. There is an amplitude reduction of the wavefields of all viscoacoustic equations compared to the trace generated by the acoustic equation. This effect is natural and expected since the wave propagates for a longer time and oscillates more times. However, the phase dispersion effect occurs only for the viscoacoustic equation based on the SLS model.

Gas chimney

The Gas Chimney constitutes a minor clipping of the BP model (Billette & Brandsberg-Dahl, 2005). Figure 3a and Figure 3b illustrate the velocity and reflectivity, respectively. The density and Q factor were calculated by Gardner relation (Gardner et al., 1974) and empirical equation $Q = 3.516 \times v^{2.2} \times 10^{-6}$ (Li, 1993). These models have $9.995 \times 4 \text{ km}^2$, discretized with $n_x = 995$ and $n_z = 402$ samples.

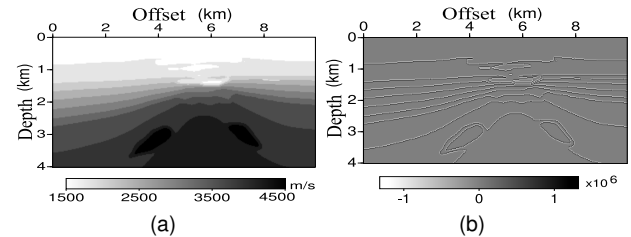


Figure 3 – Gas chimney model: velocity (a). Reflectivity(b).

Figure 9a shows all the seismograms for the analyzed viscoacoustic equations. The Gas Chimney model has a low Q factor anomaly, the upper central part of the model (Figures 3a). Its effect is notable in seismograms, presenting a significant energy loss, mainly for the Maxwell model. Analyzing the red dashed circle, we notice that the dissipative effect is not as strong as the region for the longer times indicated by the arrows. Furthermore, beyond amplitude reduction, the velocity phase dispersion effect exists for the SLS equation, which causes seismic pulse distortion. The traces for the equations based on the Maxwell and KV rheological models show the dissipative effect (Figure 9). However, they are not displaced, characterizing the non-occurrence of the dispersive effect because these viscoacoustic equations do not consider the dispersion phenomena.

We compared the wavefront propagation instants for 0.7 s and 1.2 s times between acoustic and viscoacoustic modeling. We see in Figure 10a, at 0.7 s, the wavefronts are still at the top of the Gas Chimney. However, as the wave propagates and passes through the Gas chimney, there are substantial loss of amplitude of the waves in the viscoacoustic case (as seen at 1.2 s in Figure 10a). We observe the effects of dissipation and dispersion in-depth traces for the two-time instants presented in Figures 10b.

Note in $0.7 s$ (Figure 10b), the dissipation phenomenon already occurs in all equations viscoacoustic, and soft dispersive only for the SLS equation. At $1.2 s$ time, the phase dispersion becomes higher for SLS model.

SEAM

The 2-D SEAM model is based on a deep water model of the Gulf of Mexico, containing a salt body in the central region. This model has spatial dimensions of $35km$ in the East-West direction and $15km$ in-depth, spaced every $dx = 20m$ and $dz = 20m$, respectively. In Figure 4a and b, we have the P-wave and the S-wave velocity model.

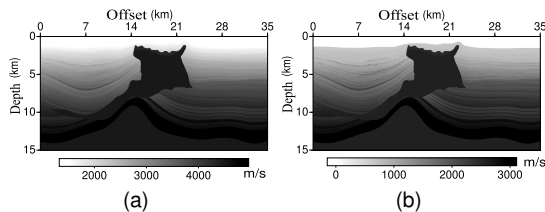


Figure 4 – SEAM model: P-velocity (a), S-velocity (b).

We generated observed viscoelastic data with 200 shots, spaced every $175m$, peak frequency of $12 Hz$, and recording time of $10s$. Figures 11a, 11b, and 11c show three shots at offset $0.175 km$, $17.51 km$, and $34.84 km$, respectively. Figures 12a, 12b, and 12c show the result of the RTM images for the forward and adjoint equations based on the SLS, Maxwell, and KV model, respectively. Because SLS forward and adjoint equations contemplate the effects of dissipation and dispersion, it is evident that the SLS RTM image has the highest resolution (Figure 12a), showing the salt flank regions better illuminated and reflectors better delineated than the RTM images based on the Maxwell (Figure 12b) and KV (Figure 12c) rheological models. Furthermore, we can see that the RTM image from the KV model (Figure 12c) is better illuminated than the RTM from the Maxwell model (Figure 12b).

Conclusions

We performed physical-numerical experiments considering velocity, quality factor, and density models with different complexities, explaining in detail the behavior and characteristics of each equation. Unlike the equations based on the Maxwell and KV models, the SLS equations can reasonably simulate the energy dissipation and phase dispersion phenomena in the forward modeling stage. They can also correct these effects in the reverse propagation stage through adjoint modeling, as evidenced in the results of RTM images. On the other hand, we note that the equations based on Maxwell and KV rheological models are most dissipative because they mainly simulate the energy loss effect.

Acknowledgements

This study was financed by the project PIE00005/2016 of Infrastructure Edictal of FAPESB 003/2015 and was financed in part by the Coordenação de Aperfeiçoamento de Pessoal de Nível Superior-Brasil (CAPES)-Finance Code 001.

We wish to thank the Supercomputing Center for Industrial Innovation at SENAI CIMATEC for the support in this research, and INCT-GP/CNPq for financial support.

References

- Billette, F. & Brandsberg-Dahl, S., 2005. The 2004 bp velocity benchmark, in: 67th EAGE Conference & Exhibition, European Association of Geoscientists & Engineers, cp-1.
- Carcione, J. M., 2014. Wave Fields in Real Media: Wave Propagation in Anisotropic, Anelastic, Porous and Electromagnetic Media, Elsevier.
- Carcione, J. M., Kosloff, D. & Kosloff, R., 1988. Wave propagation simulation in a linear viscoelastic medium, *Geophysical Journal International*, vol. 95(3): 597–611.
- Deng, F. & McMechan, G. A., 2007. True-amplitude prestack depth migration, *Geophysics*, vol. 72(3): S155–S166.
- Dutta, G. & Schuster, G. T., 2014. Attenuation compensation for least-squares reverse time migration using the viscoacoustic-wave equation, *Geophysics*, vol. 79(6): S251–S262.
- Gardner, G., Gardner, L. & Gregory, A., 1974. Formation velocity and density—the diagnostic basics for stratigraphic traps, *Geophysics*, vol. 39(6): 770–780.
- Kukreja, N. et al., 2018. High-level python abstractions for optimal checkpointing in inversion problems, arXiv preprint arXiv:1802.02474.
- Li, Q., 1993. High resolution seismic data processing, Petroleum Industry Press, China, vol. 37: 38.
- Louboutin, M. et al., 2018. Devito: an embedded domain-specific language for finite differences and geophysical exploration, arXiv preprint arXiv:1808.01995.
- Plessix, R.-E., 2006. A review of the adjoint-state method for computing the gradient of a functional with geophysical applications, *Geophysical Journal International*, vol. 167(2): 495–503.
- Ren, Z., Liu, Y. & Zhang, Q., 2014. Multiscale viscoacoustic waveform inversion with the second generation wavelet transform and adaptive time-space domain finite-difference method, *Geophysical Journal International*, vol. 197(2): 948–974.
- Robertsson, J. O., Blanch, J. O. & Symes, W. W., 1994. Viscoelastic finite-difference modeling, *Geophysics*, vol. 59(9): 1444–1456.
- Schiessel, H., Metzler, R., Blumen, A. & Nonnenmacher, T., 1995. Generalized viscoelastic models: their fractional equations with solutions, *Journal of physics A: Mathematical and General*, vol. 28(23): 6567.
- Walcott, R., 1970. Flexural rigidity, thickness, and viscosity of the lithosphere, *Journal of Geophysical Research*, vol. 75(20): 3941–3954.

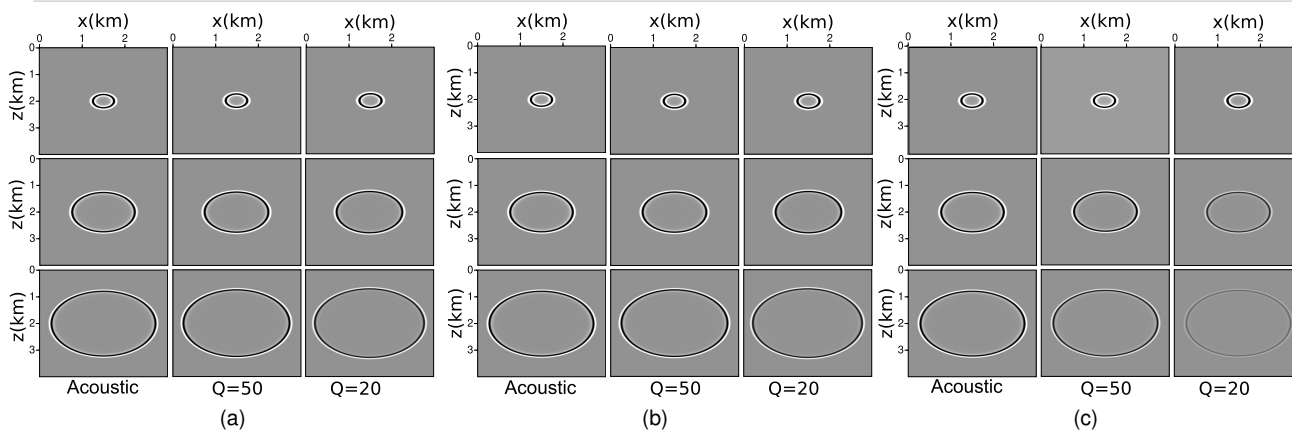


Figure 5 – Snapshots showing an expanding wavefront at different instances of time for the equations: (a) SLS, (b) KV, (c) Maxwell.

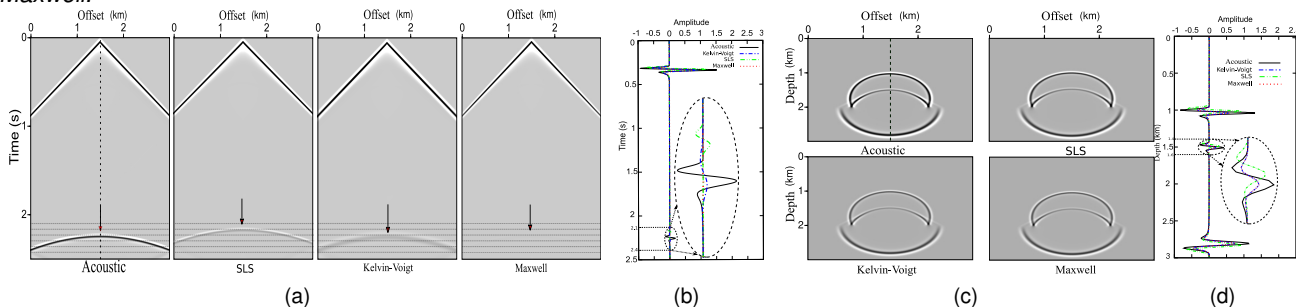


Figure 6 – Seismograms comparison, for two-layer model, between acoustic and viscoacoustic cases (a) and vertical traces comparison at 1 km (b) Snapshots comparison, for two-layer model, between acoustic and viscoacoustic cases at instances of 0.5 s (c) and vertical traces comparison at 1.5 km (d).

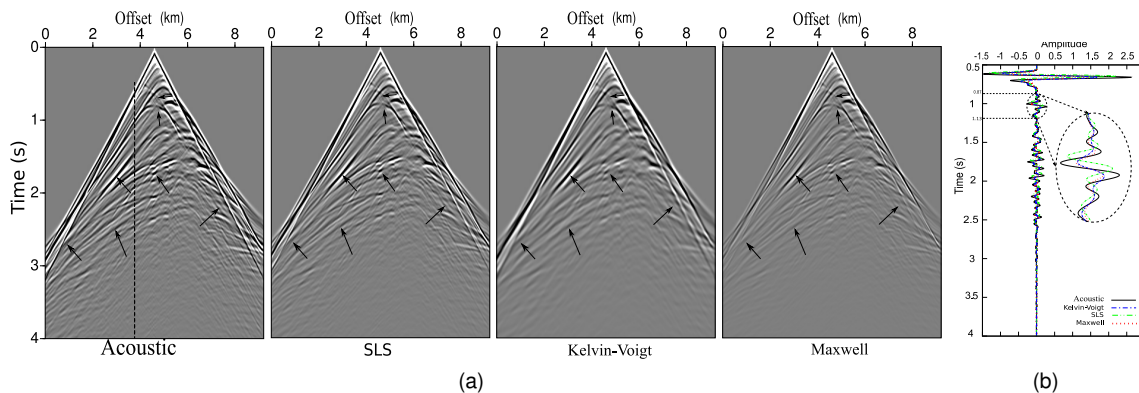


Figure 7 – Marmousi model: seismograms comparison among acoustic, SLS, KV, and Maxwell equations (a) and traces comparison at 3.75 km (b).

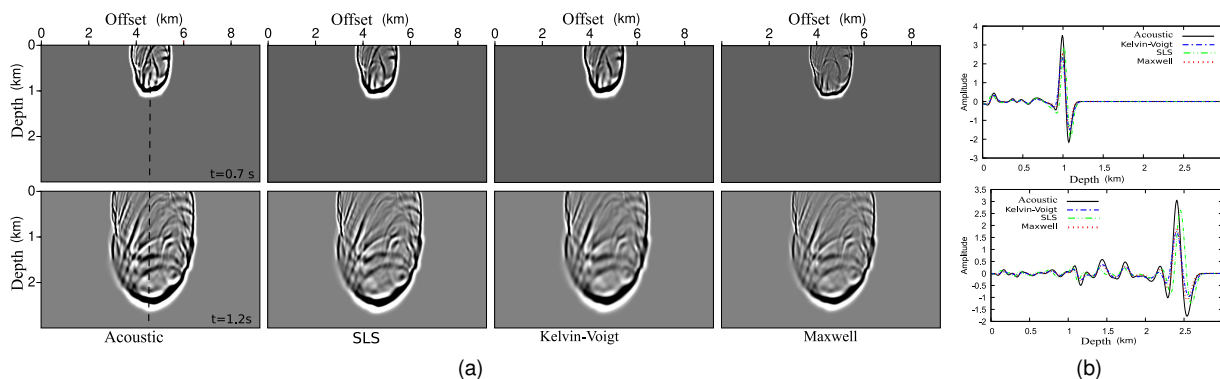


Figure 8 – Marmousi model: snapshots comparison between acoustic and viscoacoustic cases at instances of 0.7 and 1.2 s (a). Traces comparison at offset 4.6 km at instances: 0.7 s and 1.2 s (b).

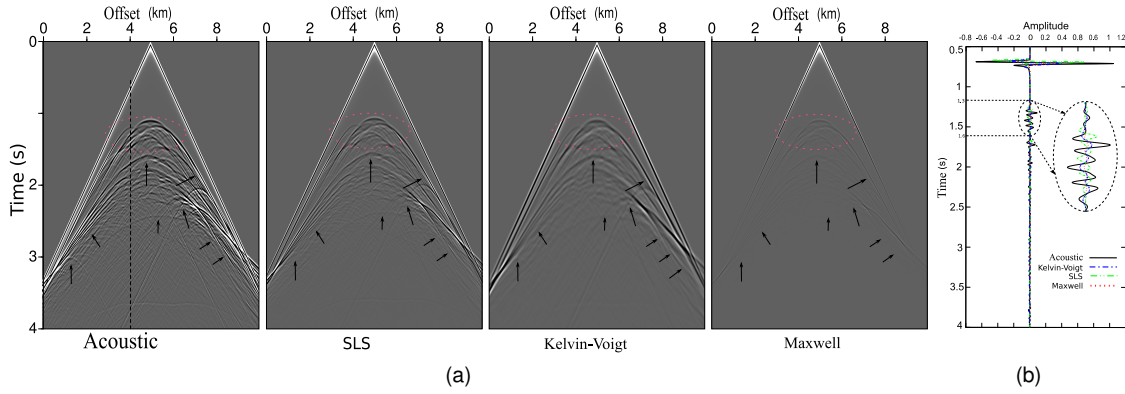


Figure 9 – Gas chimney model: seismograms comparison among acoustic, SLS, KV and Maxwell equations (a), and traces comparison at 3.75 km (b).

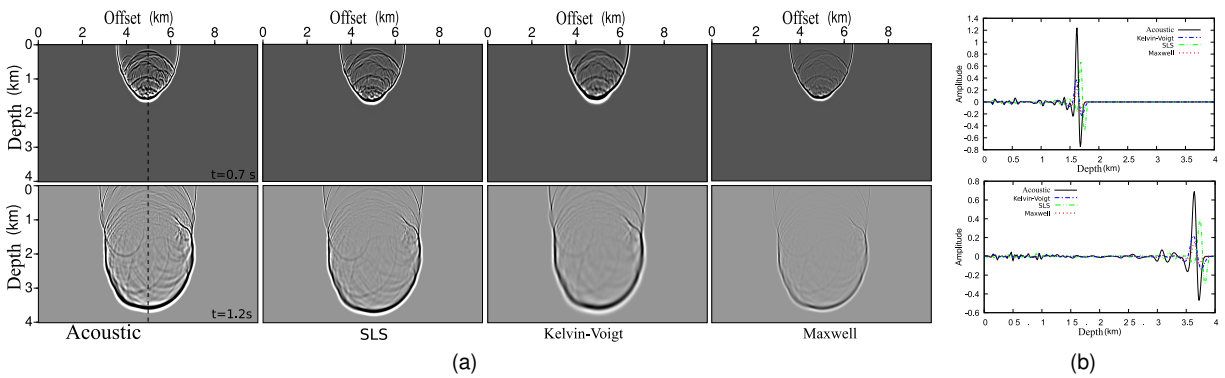


Figure 10 – Gas chimney model: snapshots comparison between acoustic and viscoacoustic cases at instances of 0.7 and 1.2 s (a). Traces comparison at offset 4.6 km at instances: 0.7 s (b) and 1.2 s (c).

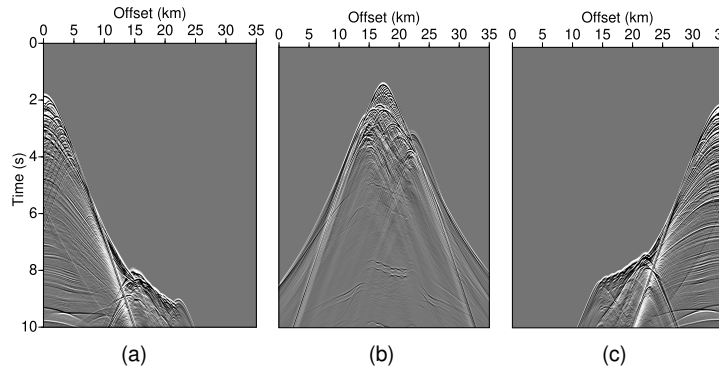


Figure 11 – SEAM shots generated at offset: = 0.175 km (a), = 17.51 km (b), and offset = 34.84 km (c).

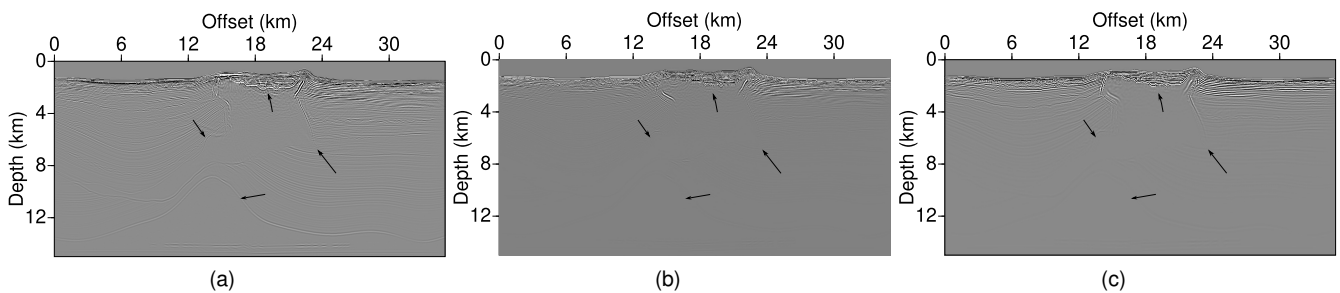


Figure 12 – SEAM model: viscoacoustic RTM applied to the viscoelastic dataset using viscoacoustic adjoint equation based on the rheological model: SLS (a), Maxwell (b), and KV (c).